Understanding Early Indicators of Critical Transitions in Power Systems From Autocorrelation Functions

Goodarz Ghanavati, *Student Member, IEEE*, Paul D. H. Hines, *Member, IEEE*, Taras I. Lakoba, and Eduardo Cotilla-Sanchez, *Member, IEEE*

Abstract—Many dynamical systems, including power systems, recover from perturbations more slowly as they approach critical transitions—a phenomenon known as critical slowing down. If the system is stochastically forced, autocorrelation and variance in time-series data from the system often increase before the transition, potentially providing an early warning of coming danger. In some cases, these statistical patterns are sufficiently strong, and occur sufficiently far from the transition, that they can be used to predict the distance between the current operating state and the critical point. In other cases CSD comes too late to be a good indicator. In order to better understand the extent to which CSD can be used as an indicator of proximity to bifurcation in power systems, this paper derives autocorrelation functions for three small power system models, using the stochastic differential algebraic equations (SDAE) associated with each. The analytical results, along with numerical results from a larger system, show that, although CSD does occur in power systems, its signs sometimes appear only when the system is very close to transition. On the other hand, the variance in voltage magnitudes consistently shows up as a good early warning of voltage collapse.

Index Terms—Autocorrelation function, bifurcation, critical slowing down, phasor measurement units, power system stability, stochastic differential equations.

I. INTRODUCTION

THERE is increasing evidence that time-series data taken from stochastically forced dynamical systems show statistical patterns that can be useful in predicting the proximity of a system to critical transitions [1], [2]. Collectively this phenomenon is known as Critical Slowing Down, and is most easily observed by testing for autocorrelation and variance in time-series data. Increases in autocorrelation and variance have been shown to give early warning of critical transitions in climate models [3], ecosystems [4], the human brain [5] and electric power systems [6]–[8].

Scheffer *et al.* [1] provide some explanation for why increasing variance and autocorrelation can indicate proximity to a critical transition. They illustrate that increasing autocorrelation results from the system returning to equilibrium more slowly after perturbations, and that increased variance results

from state variables spending more time further away from equilibrium. Reference [9] uses the mathematical theory of the stochastic fast-slow dynamical systems and the Fokker-Planck equation to explain the use of autocorrelation and variance as indicators of CSD.

While CSD is a general property of critical transitions [10], its signs do not always appear early enough to be useful as an early warning, and do not universally appear in all variables [10], [11]. References [10] and [11] both show, using ecological models, that the signs of CSD appear only in a few of the variables, or even not at all.

Several types of critical transitions in deterministic power system models have been explained using bifurcation theory. Reference [12] explains voltage collapse as a saddle-node bifurcation. Reference [13] describes voltage instability caused by the violation of equipment limits using limit-induced bifurcation theory. Some types of oscillatory instability can be explained as a Hopf bifurcation [14], [15]. Reference [16] describes an optimization method that can find saddle-node or limit-induced bifurcation points. Reference [17] shows that both Hopf and saddle-node bifurcations can be identified in a multimachine power system, and that their locations can be affected by a power system stabilizer.

Substantial research has focused on estimating the proximity of a power system to a particular critical transition. References [13], [18]–[20] describe methods to measure the distance between an operating state and voltage collapse with respect to slow-moving state variables, such as load. Although these methods provide valuable information about system stability, they are based on the assumption that the current network model is accurate. However, all power system models include error, both in state variable estimates and network parameters, particularly for areas of the network that are outside of an operator's immediate control.

An alternate approach to estimating proximity to bifurcation is to study the response of a system to stochastic forcing, such as fluctuations in load, or variable production from renewable energy sources. To this end, a growing number of papers study power system stability using stochastic models [21]–[26]. Reference [21] models power systems using Stochastic Differential Equations (SDEs) in order to develop a measure of voltage security. In [24], numerical methods are used to assess transient stability in power systems, given fluctuating loads and random faults. Reference [25] uses the Fokker-Planck equation to calculate the probability density function (PDF) for state variables in a single machine infinite bus system (SMIB), and uses the time evolution of this PDF to show how random load fluctuations affect system stability. In [26], an analytical method to compute bounds on the distribution of system states or bounds on

probabilities of different events of interest in stochastic power systems is presented. Reference [27] proposes a systematic approach to model power systems as continuous stochastic differential-algebraic equations.

The results above clearly show that power system stability is affected by stochastic forcing. However, they provide little information about the extent to which CSD can be used as an early warning of critical transitions given fluctuating measurement data. Given the increasing availability of high-sample-rate synchronized phasor measurement unit (PMU) data, and the fact that insufficient situational awareness has been identified as a critical contributor to recent large power system failures (e.g., [28], [29]) there is a need to better understand how statistical phenomena, such as CSD, might be used to design good indicators of stress in power systems.

Results from the literature on CSD suggest that autocorrelation and variance in time-series data increase before critical transitions. Empirical evidence for increasing autocorrelation and variance is provided for an SMIB and a 9-bus test case in [6]. Reference [30] shows that voltage variance at the end of a distribution feeder increases as it approaches voltage collapse. However, the results do not provide insight into autocorrelation. To our knowledge, only [7], [8] derive approximate analytical autocorrelation functions (from which either autocorrelation or variance can be found) for state variables in a power system model, which is applied to the New England 39 bus test case. However, the autocorrelation function in [7], [8] is limited to the operating regime very close to the threshold of system instability. Furthermore, there is, to our knowledge, no existing research regarding which variables show the signs of CSD most clearly in power system, and thus which variables are better indicators of proximity to critical transitions. In [31], the authors derived the general autocorrelation function for the stochastic SMIB system. This paper extends the SMIB results in [31], and studies two additional power system models using the same analytical approach. Also, this paper includes new numerical simulation results for two multi-machine systems, which illustrate insights gained from the analytical work.

Motivated by the need to better understand CSD in power systems, the goal of this paper is to describe and explain changes in the autocorrelation and variance of state variables in several power system models, as they approach bifurcation. To this end, we derive autocorrelation functions of state variables for three small models. We use the results to show that CSD does occur in power systems, explain why it occurs, and describe conditions under which autocorrelation and variance signal proximity to critical transitions. The remainder of this paper is organized as follows. Section II describes the general mathematical model and the method used to derive autocorrelation functions in this paper. Analytical solutions and illustrative numerical results for three small power systems are presented in Sections III, IV and V. In Section VI, the results of numerical simulations on two multi-machine power system models including the New England 39 bus test case are presented. Finally, Section VII summarizes the results and contributions of this paper.

II. SOLUTION METHOD FOR AUTOCORRELATION FUNCTIONS

In this section, we present the general form of the Stochastic Differential Algebraic Equations (SDAEs) used to model the three systems studied in this paper. Then, the solution of the SDAEs and the expressions for autocorrelations and variances of both algebraic and differential variables of the systems are presented. Finally, the method used for simulating the SDAEs numerically is described.

A. The Model

All three models studied analytically in this paper include a single second-order synchronous generator. These systems can be described by the following SDAEs:

$$\ddot{\delta} + 2\gamma\dot{\delta} + F_1(\delta, \underline{y}, \eta) = 0 \tag{1}$$

$$\underline{F_2}(\delta, \underline{y}, \eta) = 0 \tag{2}$$

where δ is angle of the synchronous generator's rotor relative to a synchronously rotating reference axis, $\underline{y}$ is the vector of algebraic variables, γ is the damping coefficient, $F_1, \underline{F_2}$ form a set of nonlinear algebraic equations of the systems, and η is a Gaussian random variable. η has the following properties:

$$\mathrm{E}\left[\eta(t)\right] = 0 \tag{3}$$

$$\mathrm{E}\left[\eta(t)\eta(s)\right] = \sigma_\eta^2 \cdot \delta_I(t - s) \tag{4}$$

where t, s are two arbitrary times, σ_η^2 is the intensity of noise, and δ_I represents the unit impulse (delta) function (which should not be confused with the rotor angle δ).

Equation (4) implies that we model the noise as having zero correlation time. In practical power systems, such noise originates from stochastic changes from loads and generators, as well as electromagnetic interferences, which occur over many time scales. To our knowledge, no empirical studies have quantified the spectral density, or correlation time, of fluctuations in power systems. In this paper, we assume that the spectral density of noise sources is flat over a certain frequency range, while acknowledging that this model is likely to have limitations. The higher end of the frequency range of interest is set by the sampling rate of the PMU, which is commonly 30 Hz. (Note that this is higher than the highest frequency of the system oscillations, which in our examples is in the range 1–10 Hz.) The lower end of the frequency range is set by the length of our simulated time window, which is 2 minutes, corresponding to a frequency of about 0.01 Hz. If one were to measure for CSD in a practical power system one would want to look at the statistical properties of data with a similar window length. Following the methods in [3], the window of data would be initially low-pass filtered to remove slow trends. This would ensure that the resulting data stream has zero mean, as does η in (3). The detrended dataset would retain the important oscillations that might indicate instability (typically well above 0.01 Hz), but discard slower trends. Thus, the noise model described by (3) and (4) is based on the assumption that the spectral density of noise sources is nearly constant over the frequency range of 0.01 Hz to 30 Hz. For this model to be accurate, the correlation time of the noise needs to be somewhat smaller than 1/30 s. Our numerical simulations, which use a time step size of 0.01 s, inject noise at each time step, thus implicitly assuming that the correlation time of the noise is 0.01 s (see the discussion after (20) and Section II-D). It should be noted that other studies [27], [32] have used noise models in which the noise spectral density falls off at frequencies above approximately 1 Hz, rather than our value of 30 Hz. It is likely that, as assumed in [27], [32], there is some frequency dependence in the spectral density of empirical measurements from power systems. However, the exact structure of the noise

is yet to be verified empirically. Future work is needed to determine the impact of frequency dependence (or, equivalently, the noise's finite correlation time) on the results presented in this paper.

In order to solve (1) and (2) analytically, we linearized F_1 and $\underline{F_2}$ around the stable equilibrium point. Then (1) and (2) were combined into a single damped harmonic oscillator equation with stochastic forcing:

$$\Delta\ddot{\delta} + 2\gamma\Delta\dot{\delta} + \omega_0^2\Delta\delta = -f\eta \qquad (5)$$

where ω_0 is the undamped angular frequency of the oscillator, f is a constant, and $\Delta\delta = \delta - \delta_0$ is the deviation of the rotor angle from its equilibrium value. Both ω_0 and f change with the system's equilibrium operating state. Equation (5) can be written as a multivariate Ornstein-Uhlenbeck process [33]:

$$\dot{\underline{z}}(t) = A\underline{z}(t) + B\begin{bmatrix} 0 \\ \eta(t) \end{bmatrix} \qquad (6)$$

where $\underline{z} = [\Delta\delta \ \Delta\dot{\delta}]^T$ is the vector of differential variables, $\Delta\dot{\delta}$ is the deviation of the generator speed from its equilibrium value, and A and B are constant matrices:

$$A = \begin{bmatrix} 0 & 1 \\ -\omega_0^2 & -2\gamma \end{bmatrix} \qquad (7)$$

$$B = \begin{bmatrix} 0 & 0 \\ 0 & -f \end{bmatrix} \qquad (8)$$

Given (7), the eigenvalues of A are $-\gamma \pm \sqrt{\gamma^2 - \omega_0^2}$. At $\omega_0 = 0$, one of the eigenvalues of matrix A becomes zero, and the system experiences a saddle-node bifurcation.

Equation (5) can be interpreted in two different ways: using either Itô SDE and Stratonovich SDEs. Here, we use the Stratonovich interpretation [34], where noise has finite, albeit very small, correlation time [33]. The reason why we chose the Stratonovich interpretation is that it allows the use of ordinary calculus, which is not possible with the Itô interpretation.

If $\gamma < \omega_0$ (which holds until very close to the bifurcation in two of our systems), the solution of (6) is [35]:

$$\Delta\delta(t) = f \cdot \int_{-\infty}^{t} \exp\left(\gamma(t'-t)\right)\eta(t')$$
$$\cdot \frac{\sin\left(\omega'(t'-t)\right)}{\omega'}dt' \qquad (9)$$

$$\Delta\dot{\delta}(t) = -f \cdot \int_{-\infty}^{t} \exp\left(\gamma(t'-t)\right)\eta(t')$$
$$\cdot \frac{\sin\left(\omega'(t'-t) + \phi\right)\omega_0}{\omega'}dt' \qquad (10)$$

where $\omega' = \sqrt{\omega_0^2 - \gamma^2}$ and $\phi = \arctan(\omega'/\gamma)$.

In the system in Section IV, $\omega_0 = 0$ for all system parameters, so the condition $\gamma < \omega_0$ does not hold. Therefore, the solution of (5) in that system is different from (9), (10):

$$\Delta\dot{\delta} = -f\int_{-\infty}^{t} \exp\left(-2\gamma(t-t')\right)\eta(t')dt' \qquad (11)$$

B. Autocorrelation and Variance of Differential Variables

Given that the eigenvalues of A have negative real part (because $\gamma > 0$), one can calculate the stationary variances and autocorrelations of $\Delta\delta$ and $\Delta\dot{\delta}$ using (3), (4), (9) and (10). The variances of the differential variables are as follows:

$$\sigma_{\Delta\delta}^2 = \frac{f^2\sigma_\eta^2}{4\gamma\omega_0^2} \qquad (12)$$

$$\sigma_{\Delta\dot{\delta}}^2 = \frac{f^2\sigma_\eta^2}{4\gamma} \qquad (13)$$

If $\gamma < \omega_0$, their normalized autocorrelation functions are:

$$\frac{\mathrm{E}\left[\Delta\delta(t)\Delta\delta(s)\right]}{\sigma_{\Delta\delta}^2} = \exp(-\gamma\Delta t)\frac{\omega_0}{\omega'} \cdot \sin(\omega'\Delta t + \phi) \qquad (14)$$

$$\frac{\mathrm{E}\left[\Delta\dot{\delta}(t)\Delta\dot{\delta}(s)\right]}{\sigma_{\Delta\dot{\delta}}^2} = \exp(-\gamma\Delta t)\frac{-\omega_0}{\omega'} \cdot \sin(\omega'\Delta t - \phi) \qquad (15)$$

where $\Delta t = t - s$ and $\omega' = \sqrt{\omega_0^2 - \gamma^2}$ as above.

If $\omega_0 = 0$, the variance of $\Delta\dot{\delta}$ can be calculated from (13) and the autocorrelation of $\Delta\dot{\delta}$ is as follows:

$$\frac{\mathrm{E}\left[\Delta\dot{\delta}(t)\Delta\dot{\delta}(s)\right]}{\sigma_{\Delta\dot{\delta}}^2} = \exp(-2\gamma\Delta t) \qquad (16)$$

C. Autocorrelation and Variance of Algebraic Variables

In order to compute the autocorrelation functions of the algebraic variables, we calculated the algebraic variables as linear functions of the differential variable $\Delta\delta$ and the noise η, by linearizing $\underline{F_2}$ in (2):

$$\Delta y_i(t) = C_{i,1}\Delta\delta(t) + C_{i,2} \qquad (17)$$

where y_i is an algebraic variable, and $C_{i,1}, C_{i,2}$ are constants. Then, the autocorrelation of Δy_i for $t \geq s$ is:

$$\mathrm{E}\left[\Delta y_i(t)\Delta y_i(s)\right] = C_{i,1}^2 \cdot \mathrm{E}\left[\Delta\delta(t)\Delta\delta(s)\right]$$
$$+ C_{i,1}C_{i,2} \cdot \mathrm{E}\left[\Delta\delta(t)\eta(s)\right] + C_{i,2}^2 \cdot \mathrm{E}\left[\eta(t)\eta(s)\right] \qquad (18)$$

In deriving (18), we used the fact that $\mathrm{E}[\Delta\delta(s)\eta(t)] = 0$ since the system is causal. Equation (18) shows that, in order to calculate the autocorrelation of $\Delta y_i(t)$, it is necessary to calculate $\mathrm{E}[\Delta\delta(t)\eta(s)]$, which can be found from (9):

$$\mathrm{E}\left[\Delta\delta(t)\eta(s)\right] = -\exp(-\gamma\Delta t) \cdot \frac{f}{\omega'} \cdot \sin(\omega'\Delta t)\sigma_\eta^2 \qquad (19)$$

This shows that $\mathrm{cov}(\Delta\delta, \eta) = 0$.

In order to use (18) to compute the variance of Δy_i, we need to carefully consider our model of noise in numerical computations. According to (4), the variance of η is infinite, because the delta function is infinite at $t = s$, which would mean that the variance of Δy_i could be infinite. However, the noise in numerical simulations must have a finite variance. To determine it, we rewrite (6) as follows:

$$d\underline{z}(t) = A\underline{z}(t)dt + Bd\underline{W}(t) \qquad (20)$$

where $d\underline{W}(t) = \eta dt$ is the Wiener process. It is well-known that the variance of $dW(t)$ is $\sigma_\eta^2 dt$ [33]. In numerical simulations, $dt = \tau_{\mathrm{int}}$, where τ_{int} is the integration time step. Thus,

$E[dW_{\text{num}}^2] = \text{E}[(\eta_{\text{num}}\tau_{int})^2] = \sigma_\eta^2\tau_{\text{int}}$. Hence, $E[\eta_{\text{num}}^2] = \sigma_\eta^2/\tau_{\text{int}}$. Then from (17):

$$\sigma_{\Delta y_i}^2 = C_{i,1}^2\sigma_{\Delta\delta}^2 + C_{i,2}^2\frac{\sigma_\eta^2}{\tau_{\text{int}}} \tag{21}$$

Combining (12) and (21) results in the following:

$$\sigma_{\Delta y_i}^2 = \left(\frac{C_{i,1}^2 f^2}{4\gamma\omega_0^2} + \frac{C_{i,2}^2}{\tau_{\text{int}}}\right)\sigma_\eta^2 \tag{22}$$

Combining (12), (14), (18), (19) and (22), we calculated the normalized autocorrelation function of Δy_i:

$$\frac{\text{E}\left[\Delta y_i(t)\Delta y_i(s)\right]}{\sigma_{\Delta y_i}^2} = \exp(-\gamma\Delta t)\sin(\omega'\Delta t + \phi_{\Delta y_i})$$
$$\cdot\frac{C_{i,1}f\omega_0\sqrt{\lambda}}{\omega'\left(C_{i,1}^2 f^2 + 4C_{i,2}^2\gamma\omega_0^2\right)} \tag{23}$$

where $\lambda = \sqrt{C_{i,1}f(C_{i,1}f - 8C_{i,2}\gamma^2) + (4C_{i,2}\omega_0\gamma)^2}$, $\phi_{\Delta y_i} = \arctan(C_{i,1}f\omega'/(C_{i,1}f\gamma - 4C_{i,2}\gamma\omega_0^2))$.

D. Numerical Simulation

We numerically solved (1) and (2) using a trapezoidal ordinary differential equation solver, as follows. First, (1) was written as:

$$\dot{\underline{z}} = \underline{\mathcal{F}_1} \equiv \begin{bmatrix} z_2 \\ -2\gamma z_2 - F_1 \end{bmatrix} \tag{24}$$

where $\underline{z} = (z_1, z_2)^T$ was defined after (6). Then, (1) and (2) were discretized:

$$\underline{z}^{(n+1)} - \underline{z}^{(n)} = \frac{\tau_{int}}{2}\left(\underline{\mathcal{F}_1}^{(n)} + \underline{\mathcal{F}_1}^{(n+1)}\right) \tag{25}$$

$$0 = \underline{\mathcal{F}_2}^{(n+1)} \tag{26}$$

where τ_{int} is a fixed integration time step, $\underline{z}^{(n)}, \underline{z}^{(n+1)}$ are the solutions at times $t^{(n)} = n\tau_{int}$ and $t^{(n+1)} = (n+1)\tau_{int}$, $\underline{F}_2^{(n+1)} \equiv \underline{F}_2(\underline{z}^{(n+1)}, \underline{y}^{(n+1)}, \eta^{(n+1)})$, and similarly for $\underline{\mathcal{F}_1}^{(n)}, \underline{\mathcal{F}_1}^{(n+1)}$. The nonlinear algebraic system (25), (26) was solved by Newton's method for $\underline{z}^{(n+1)}$ and $\underline{y}^{(n+1)}$, with values $\underline{z}^{(n)}$ and $\underline{y}^{(n)}$ being known from the previous step and $\eta^{(n+1)}$ being a random variable generated at $t^{(n+1)}$. Note that $\eta^{(n)}$ and $\eta^{(n+1)}$ are uncorrelated, and, according to the discussion after (20), the variance of $\eta^{(n)}$ was $\sigma_\eta^2/\tau_{\text{int}}$. The integration time step τ_{int} was chosen to be 0.01 s, which is about ten times smaller than Δt, where Δt is the time lag for calculation of the autocorrelation.

In order to determine numerical mean values in this paper, each set of SDEs was simulated 100 times. In each case the resulting averages were compared with analytical means.

III. SINGLE MACHINE INFINITE BUS SYSTEM

Analysis of small power system models can be helpful for understanding the concepts of power system stability. The single machine infinite bus system has long been used to understand the behavior of a generator connected to a larger
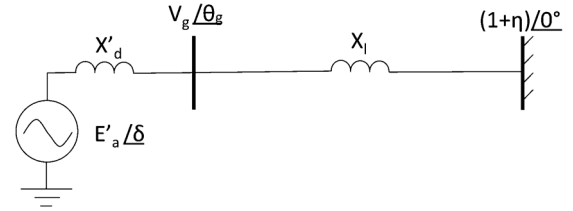

Fig. 1. Stochastic single machine infinite bus system used in Section III. The notation $V_g\underline{/\theta_g}$ represents $V_g\exp[j\theta_g]$.

system through a long transmission line. It has also been used to explore the small signal stability of synchronous machines [36] and to evaluate control techniques to improve transient stability and voltage regulation [37]. Recently, there has been increased interest in stochastic behavior of power systems, in part due to the integration of renewable energy sources. A few of these papers use stochastic SMIB models. For example, references [25], [38] studied stability in a stochastic SMIB system.

In this section, we use the autocorrelation functions derived in Section II to calculate the variance and autocorrelation of the state variables of a stochastic SMIB system. Analysis of these functions provides analytical evidence for, and insight into, CSD in a small power system.

A. Stochastic SMIB System Model

Fig. 1 shows the stochastic SMIB system. Equation (27), which combines the mechanical swing equation and the electrical power produced by the generator, fully describes the dynamics of this system:

$$M\ddot{\delta} + D\dot{\delta} + \frac{(1+\eta)E_a'}{X}\sin(\delta) = P_m \tag{27}$$

where ($\eta \sim \mathcal{N}(0, 0.01)$) is a white Gaussian random variable added to the voltage magnitude of the infinite bus to account for the noise in the system, M and D are the combined inertia constant and damping coefficient of the generator and turbine, and E_a' is the transient emf. The reactance X is the sum of the generator transient reactance (X_d') and the line reactance (X_l), and P_m is the input mechanical power. The values of parameters used in this section are given below:

$$D = 0.03\,\frac{\text{pu}}{\text{rad/s}},\; H = 4\,\frac{\text{MW.s}}{\text{MVA}},\; X_d' = 0.15\,\text{pu},$$
$$X_l = 0.2\,\text{pu},\; \omega_s = 2\pi\cdot 60\,\text{rad/s}$$

Note that $M = 2H/\omega_s$, where H is the inertia constant in seconds, and ω_s is the rated speed of the machine. The generator and the system base voltage levels are 13.8 kV and 115 kV, and both the generator and system per unit base are set to 100 MVA. The generator transient reactance $X_d' = 0.15\cdot(13.8/115)^2$ pu, on the system pu base. The third term on the left-hand side of (27) is the generator's electrical power (P_g).

In order to test the system at various load levels, we solved the system for different equilibria, with the generator's mechanical and electrical power equal at each equilibrium:

$$P_m = P_{g0} = \frac{E_a'}{X}\sin(\delta_0) \tag{28}$$

where δ_0 is the equilibrium value of the generator's rotor angle.

B. Autocorrelation and Variance

In this section, we calculate the autocorrelation and variance of the algebraic and differential variables of this system using the method in Section II. Equations (1) and (2) describe this system for which the following equalities hold:

$$\gamma = \frac{D}{2M}; \ \omega_0 = \sqrt{\frac{E'_a \cos \delta_0}{MX}}; \underline{y} = [V_g \ \theta_g]^T \qquad (29)$$

$$f = \frac{P_{g0}}{M}; \ F_1(z, \underline{y}, \eta) = \frac{\left(\frac{(1+\eta)E'_a}{X} \sin \delta - P_m\right)}{M} \qquad (30)$$

where $\Delta V_g = V_g - V_{g0}, \Delta \theta_g = \theta_g - \theta_{g0}$ are the deviations of, respectively, the generator terminal busbar's voltage magnitude and angle from their equilibrium values. Equations (29) and (30) show that f increases, while ω_0 decreases, with δ_0.

In order to calculate the algebraic equations, which form $\underline{F_2}(\delta, y, \eta)$ in (2), we wrote Kirchhoff's current law at the generator's terminal:

$$\frac{E'_a e^{j\delta} - V_g e^{j\theta_g}}{jX'_d} + \frac{1 + \eta - V_g e^{j\theta_g}}{jX_l} = 0 \qquad (31)$$

Separating the real and imaginary parts in (31) gives:

$$V_g \sin(\theta_g) = \alpha E'_a \sin(\delta) \qquad (32)$$

$$V_g \cos(\theta_g) = \alpha E'_a \cos(\delta) + (1 + \eta)(1 - \alpha) \qquad (33)$$

where $\alpha = X_l/(X_l + X'_d)$. Equations (32) and (33) combine to make $\underline{F_2}(\delta, y, \eta)$ in (2).

Linearizing (32) and (33) yields the coefficients in (17), which are necessary for calculating the autocorrelation and variance of the algebraic variables ($y_1 = \Delta V_g, y_2 = \Delta \theta_g$):

$$C_{1,1} = \alpha E'_a \sin(\theta_{g0} - \delta_0) \qquad (34)$$

$$C_{1,2} = (1 - \alpha) \cos(\theta_{g0}) \qquad (35)$$

$$C_{2,1} = \alpha E'_a \cos(\theta_{g0} - \delta_0) \qquad (36)$$

$$C_{2,2} = -(1 - \alpha) \sin(\theta_{g0}) \qquad (37)$$

Fig. 2 shows the decrease of ω', which is the imaginary part of the eigenvalues of A in (7), with P_m. Note that the bifurcation occurs at $b = 5$ pu. This figure illustrates how it can be difficult to accurately foresee a bifurcation by computing the eigenvalues of a system (as in, e.g., [18]), if there is noise in the measurements feeding the calculation. The value of $\omega' \sim (P_m - b)^{1/4}$ does not decrease by a factor of two (compared to its value at $P_m = 1.0$ pu) until $P_m = 4.83$ pu (only <3.4% away from the bifurcation). It decreases by another factor of two at $P_m = 4.99$ pu (0.2% away from the bifurcation). Also, note that the real part of the eigenvalues equals $-\gamma$ until very close to the bifurcation (0.1% away from the bifurcation), so it does not provide a useful indication of proximity to the bifurcation either, Thus, one can confidently predict from ω' the imminent occurrence of the bifurcation only very near it, which may be too late to avert it. On the other hand, we will demonstrate below that for this system, autocorrelation functions can provide substantially more advanced warning of the bifurcation.

Using autocorrelation as an early warning sign of a bifurcation requires one to carefully select a time lag, $\Delta t = t - s$, such that changes in autocorrelation are observable. To understand the impact of different time lags, we computed the autocorrelation function of $\Delta \delta$ (see Fig. 3). From (14), the autocorrelation of $\Delta \delta$ crosses zero at $\Delta t_0 = (2\pi - \phi)/\omega'$. We note that choosing Δt close to, but below, Δt_0 allows one to observe a
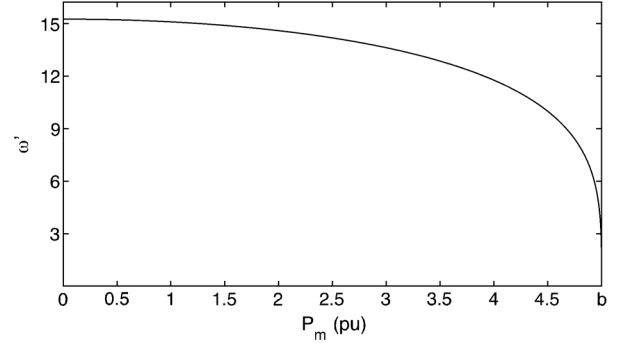

Fig. 2. The decrease of ω' with P_m in the SMIB system. Near the bifurcation, ω' is very sensitive to changes in P_m. In this figure, and most that follow, b is the value of the bifurcation parameter (P_m in this system) at the bifurcation.
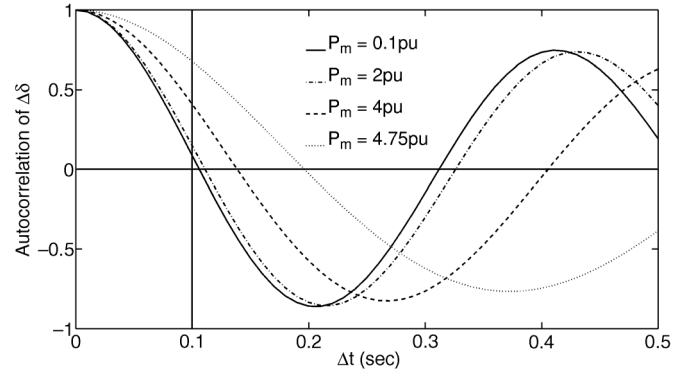

Fig. 3. Autocorrelation function of $\Delta \delta$. $\Delta t = 0.1$ s is close to 1/4 of the smallest period of the function for all values of P_m.

monotonic increase of autocorrelation as P_m increases. Indeed, for $\Delta t > \Delta t_0$, autocorrelation may not increase monotonically, or the autocorrelation for some values of P_m may be negative. For example, in Fig. 3 for $\Delta t = 0.3$ s, the autocorrelation decreases first and then increases with P_m. On the other hand, for Δt considerably smaller than Δt_0, the increase of the autocorrelation may not be large enough to be measurable. In Fig. 3, the curves converge as $\Delta t \to 0$. Given that the smallest period of oscillation ($T = 2\pi/\omega'$) in this system is 0.41 s, we chose $\Delta t = 0.1$ s for the autocorrelation calculations in this section.

Using (12)–(15), we calculated the variance and autocorrelation of $\Delta \delta$, $\dot{\Delta \delta}$ at different operating points. In Fig. 4, these analytical results are compared with the numerical ones. To initialize the numerical simulations, we assumed that $V_{g0} = 1$ pu and solved for E'_a in (32), (33) to obtain $V_g = V_{g0}$ (for $\eta = 0$). We chose the integration step size $\tau_{int} = 0.01$ s, which is much shorter than the the smallest period of oscillation ($T = 0.41$ s) and the time lag Δt. The numerical results are shown for the range of bifurcation parameter values for which the numerical solutions were stable.

In order to determine if variance and autocorrelation measurably increase as load approaches the bifurcation, we compared a base load level (the normal operating condition of the system) with a load level that is high, and closer to the bifurcation, but still some distance from the bifurcation (far enough that an operator would have time to take precautionary control actions). Since our aim is to study early warning signs of the bifurcation, we use the differences between these two states as an indication of whether particular variables provide observable early warning. While different load values for these two points could be chosen for different systems, in this paper we assume that
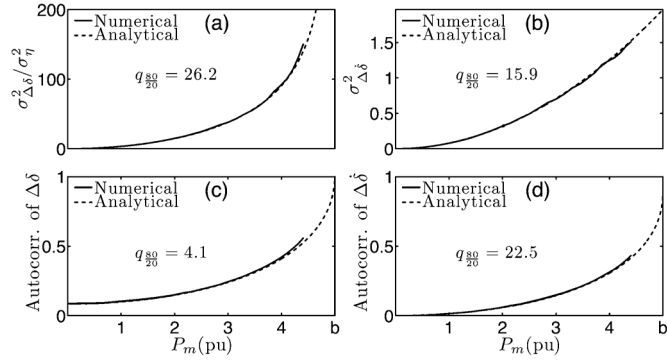
Fig. 4. Panels a,b show the variances of $\Delta\delta, \Delta\dot{\delta}$ versus mechanical power (P_m) values. Panels c,d show the autocorrelations of $\Delta\delta, \Delta\dot{\delta}$ versus mechanical power (P_m) values. The autocorrelation values are normalized by dividing by the variances of the variables.

the base level is 20% of the load at the bifurcation point, and the high load level is at 80%Therefore, we computed the ratio of each statistic when load is at 80% of the bifurcation value to the value when load is at 20% of b. This ratio, $q_{80/20}$ in Fig. 4, is defined as follows:

$$q_{\frac{80}{20}} = \frac{\text{Autocorrelation of } u \text{ or } \sigma_u^2|_{P_m=0.8b}}{\text{Autocorrelation of } u \text{ or } \sigma_u^2|_{P_m=0.2b}} \quad (38)$$

where u is the plot's variable. In subsequent figures, $q_{80/20}$ is defined similarly.

Fig. 4 shows that the variance of both $\Delta\delta$ and $\Delta\dot{\delta}$ increases substantially with P_m, and thus appears to be a good warning sign of the bifurcation. However, the two variances grow with different rates. (This becomes clear when comparing the ratios $q_{80/20}$ for $\Delta\delta$ and $\Delta\dot{\delta}$.) The difference becomes even more noticeable near the bifurcation where the variance of $\Delta\delta$ increases much faster than the variance of $\Delta\dot{\delta}$. This is caused by the term ω_0^2 in the denominator of the expression for the variance of $\Delta\delta$ in (12). In Fig. 4, the autocorrelation of $\Delta\delta$ and $\Delta\dot{\delta}$ increases with P_m. Similar to the variance, the autocorrelation is a good early warning sign of the bifurcation. Comparing Fig. 4 with Fig. 2 (where an equivalent $q_{80/20}$ would be 1.28) shows that the autocorrelations and variances of $\Delta\delta$ and $\Delta\dot{\delta}$ provide a substantially stronger early warning sign, relative to using eigenvalues to estimate the distance to bifurcation in this system.

The results for the algebraic variables are mainly similar. Fig. 5 show the variance and autocorrelation of $\Delta V_g, \Delta\theta_g$ as a function of load. In Fig. 5, the variance of ΔV_g decreases with P_m until the system gets close to the bifurcation, while the variance of $\Delta\theta_g$ increases with P_m even if the system is far from the bifurcation. The autocorrelations of both ΔV_g and $\Delta\theta_g$ in Fig. 5 increase with P_m. However, the ratio $q_{80/20}$ in (38) is much larger for ΔV_g than for $\Delta\theta_g$. This is caused by the autocorrelation of ΔV_g being very close to zero for small values of P_m.

C. Discussion

These results can be better understood by observing the trajectory of the eigenvalues of the SMIB system (Fig. 6). Near the bifurcation, the eigenvalues are very sensitive to changes in the bifurcation parameter. As a result, the system is in the overdamped regime ($\omega_0 < \gamma$) for much less than 0.1% distance in terms of P_m to the critical transition. This implies that, at least for this system, the autocorrelation function in [7], [8], is
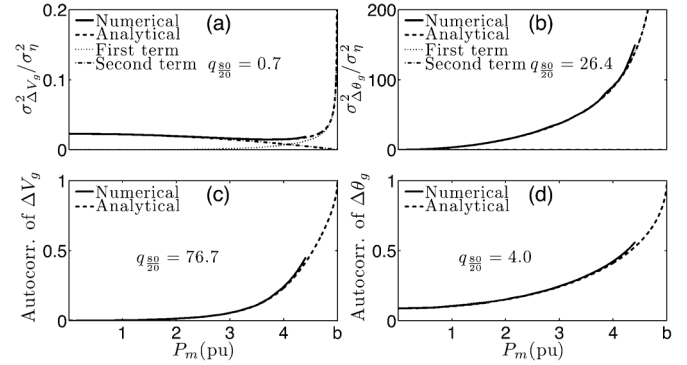

Fig. 5. Panels a,b show the variances of ΔV_g and $\Delta\theta_g$ versus mechanical power (P_m) levels. The two terms comprising the variances in (21) are also shown. Panels c,d show the autocorrelations of ΔV_g and $\Delta\theta_g$ versus P_m.
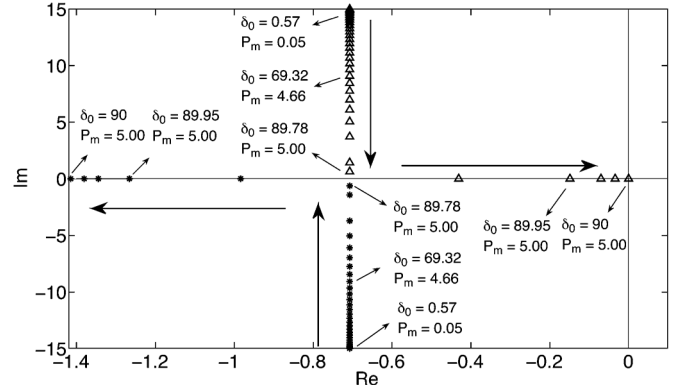

Fig. 6. Eigenvalues of the first system as the bifurcation parameter (mechanical power) is increased. The arrows show the direction of the eigenvalues' movement in the complex plane as P_m is increased. The values of P_m and δ_0 are given for several eigenvalues.

valid only when the system is within 0.1% of the saddle-node bifurcation. By considering a range of system parameters, we observed that the region where one eigenvalue determines the system dynamics is within 1.5% of the bifurcation point at most. The width of this region scales approximately with D^2, X_l and $1/H$. Because the method in [7], [8] can provide a good estimate of the autocorrelations and variances of state variables only for a very short range of the bifurcation parameter, it may not be particularly useful as an early warning sign of bifurcation.

From Figs. 4, 5, we can observe that, except for the variance of ΔV_g, the variances and autocorrelations of all state variables increase when the system is more loaded. This demonstrates that CSD occurs in this system as it approaches bifurcation, as suggested both by general results [9], and prior work for power systems [6], [7]. As an example, we calculated the variances of $\Delta\delta$ and $\Delta\dot{\delta}$ as a function of the system parameters using (12), (13) and (29):

$$\sigma_{\Delta\delta}^2 = \frac{E_a'\sigma_\eta^2}{2X^2D} \cdot \frac{\sin^2\delta_0}{\cos\delta_0} \quad (39)$$

$$\sigma_{\Delta\dot{\delta}}^2 = \frac{E_a'^2\sigma_\eta^2}{2MX^2D} \cdot \sin^2\delta_0 \quad (40)$$

It can be observed from these expressions that as the system approaches the bifurcation ($\delta_0 \longrightarrow 90$), the variable terms $(\sin^2\delta_0/\cos\delta_0), \sin^2\delta_0$ also increase. As a result, variance of $\Delta\delta, \Delta\dot{\delta}$ both increase under all conditions.

In addition to validating these prior results, several new observations can be made. For example, the signs of CSD are more

clearly observable in some variables than in others. While all of the variables show some increase in autocorrelation and variance, they are less clearly observable in ΔV_g. The variance of ΔV_g decreases with P_m slightly until the vicinity of the bifurcation. In comparison, the variance of $\Delta \theta_g$ always increases with P_m. Fig. 5 shows the two terms of the expressions for the variances of ΔV_g and $\Delta \theta_g$ in (21). The second term of the variance of $\Delta \theta_g$ is very small compared to the first term, and the first term is always dominant and growing. On the other hand, the second term of the variance of ΔV_g is more significant for small P_m. This term decreases with P_m, which can be observed from the expression for $C_{1,2}$ in (35). Accordingly, decrease of $C_{1,2}$ with P_m causes the the variance of ΔV_g to decrease with P_m until the vicinity of the bifurcation. In conclusion, the variance of $\Delta \theta_g$ is a better indicator of proximity to the bifurcation. Because the variables $\Delta \delta$ and $\Delta \dot{\delta}$ are highly correlated with $\Delta \theta_g$, their variances are also good indicators of proximity to the bifurcation.

The rate at which autocorrelation increases with P_m differs significantly in Figs. 4 and 5. In Fig. 4, the ratio $q_{80/20}$ in (38) is times larger for $\Delta \dot{\delta}$ than for $\Delta \delta$. The normalized autocorrelation functions of $\Delta \delta$ and $\Delta \dot{\delta}$ are as follows:

$$\frac{\mathrm{E}\left[\Delta\delta(t)\Delta\delta(s)\right]}{\sigma_{\Delta\delta}^2} = \exp(-\gamma\Delta t)\frac{\omega_0}{\omega'} \cdot \sin(\omega'\Delta t + \phi) \quad (41)$$

$$\frac{\mathrm{E}\left[\Delta\dot{\delta}(t)\Delta\dot{\delta}(s)\right]}{\sigma_{\Delta\dot{\delta}}^2} = \exp(-\gamma\Delta t)\frac{\omega_0}{\omega'} \cdot \sin(\omega'\Delta t + \pi - \phi) \quad (42)$$

The difference between the two functions is in the phase of the sine function which causes the values of the two autocorrelations to be different. $q_{80/20}$ is so much larger for $\Delta \dot{\delta}$ than for $\Delta \delta$ because of the time lag (Δt) used to compute autocorrelation. $\Delta t = 0.1$ s is close to the zero crossing of the autocorrelation function of $\Delta \dot{\delta}$, causing the large $q_{80/20}$. This difference illustrates the importance of choosing an appropriate time lag.

It is important to note that although the growth ratio of the autocorrelation for $\Delta \delta$ is not large compared to $\Delta \dot{\delta}$, it can be increased by subtracting a bias value from the autocorrelation values for $P_m = 0.2b$ (pu) and $P_m = 0.8b$ (pu). For example, if the value of 0.075 is subtracted from the autocorrelation values, the ratio $q_{80/20}$ increases from 4.1 to 13.0.

The results also show the nonlinearity of F_1 in (30), causes the changes in autocorrelation and variance of the system variables In [33], it is shown that the stationary time correlation matrix of (6) can be calculated using the following equation:

$$\mathrm{E}\left[\underline{Z}(t)\underline{Z}^T(s)\right] = \exp[-A\Delta t]\sigma \quad (43)$$

where σ is the covariance matrix of the state variables. Thus, the normalized autocorrelation matrix depends only on A and the time lag. One of the elements of the state matrix $(-\omega_0^2)$ in (7) changes with P_m because of the nonlinear relationship between the electrical power (P_g) and the rotor angle in F_1. Thus, in this system, CSD is caused by the nonlinearity of F_1.

IV. SINGLE MACHINE SINGLE LOAD SYSTEM

The first system illustrates how CSD can occur in a generator connected to a large power grid, through a long line. In this section we use a generator to represent the bulk grid, and look for signs of CSD caused by a stochastically varying load. Some form of the single machine single load (SMSL) model used in
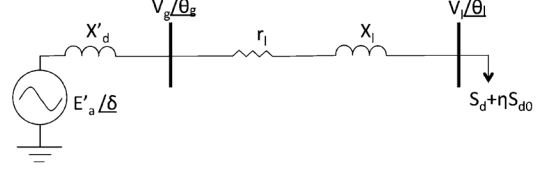

Fig. 7. Single machine single load system.

this section has been used extensively to study voltage collapse (e.g., [13], [39]).

A. Stochastic SMSL System Model

The second system (shown in Fig. 7) consists of one generator, one load and a transmission line between them. The random variable η defined in (3) and (4), is added to the load to model its fluctuations. The load consists of both active and reactive components. In order to stress the system, the baseline load S_d is increased, while keeping the noise intensity (S_{d0}) and the load's power factor constant.

A set of differential-algebraic equations comprising the swing equation and power flow equations describe this system. The swing equation and the generator's electrical power equation are given below:

$$M\ddot{\delta} + D\dot{\delta} = P_m - P_g \quad (44)$$

$$P_g = E_a'V_lG_{gl}\cos(\delta - \theta_l) + E_a'V_lB_{gl}\sin(\delta - \theta_l) + E_a'^2G_{gg} \quad (45)$$

where V_l, θ_l are voltage magnitude and angle of the load busbar, G_{gl}, G_{gg} and B_{gl} are as follows:

$$G_{gg} = -G_{gl} = \mathrm{Re}\left(\frac{1}{r_l + jX_l}\right) \quad (46)$$

$$B_{gl} = -\mathrm{Im}\left(\frac{1}{r_l + jX_l}\right) \quad (47)$$

The power flow equations at the load bus are as follows:

$$-P_d - P_{d0}\eta = E_a'V_lG_{gl}\cos(\theta_l - \delta) + E_a'V_lB_{gl}\sin(\theta_l - \delta) + V_l^2G_{ll} \quad (48)$$

$$-Q_d - Q_{d0}\eta = E_a'V_lG_{gl}\sin(\theta_l - \delta) - E_a'V_lB_{gl}\cos(\theta_l - \delta) - V_l^2B_{ll} \quad (49)$$

where $G_{ll} = G_{gg}$, $B_{ll} = -B_{gl}$, and P_{d0}, Q_{d0} are constant values. The parameters of this system are similar to the SMIB system, with the following additional parameters: $r_l = 0.025\,\Omega$, $P_{d0} = 1$ pu, $pf = 0.95$ lead, where r_l is the line's resistance and pf is the load's power factor.

In this system, V_l, $\theta_l - \delta$ are the algebraic variables, and δ, $\dot{\delta}$ are the differential variables. The algebraic (48) and (49) define V_l and $\theta_l - \delta$, which then drive δ through (44) and (45). By linearizing (45) and the power flow equations around the equilibrium, we simplified (44) to the following:

$$\Delta\ddot{\delta} + \frac{D}{M}\Delta\dot{\delta} = -\frac{C_5}{M}\eta \quad (50)$$

where C_5 is a function of the system state at the equilibrium point. The derivation of (50) and the expression for C_5 are presented in Appendix A. Comparing (5) with (50) yields:

$$\gamma = \frac{D}{2M}, \; \omega_0 = 0, \; f = \frac{C_5}{M} \quad (51)$$

The expression for the autocorrelation of $\Delta\dot{\delta}$ is given in (16). Note that the normalized autocorrelation of $\Delta\dot{\delta}$ does not change
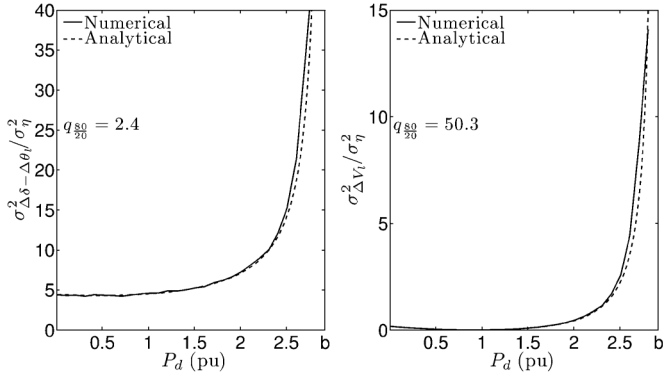
Fig. 8.   Variances of $\Delta\delta - \Delta\theta_l$ and ΔV_l for different load levels. Both variances increase with P_d as the system approaches the bifurcation.
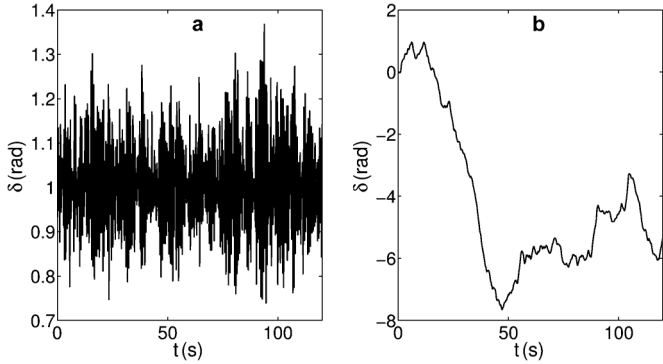

Fig. 9.   A sample trajectory of the rotor angle of (a) the SMIB system (b) the SMSL system.

with the bifurcation parameter (P_d), as it did for the SMIB system. In Appendix A, it is shown that ΔV_l and $\Delta\delta - \Delta\theta_l$ are proportional to η (see (59) and (60)). As a result, they are memoryless; the variables have zero autocorrelation.

Fig. 8 shows the analytical and numerical solutions of the variances of ΔV_l and $\Delta\delta - \Delta\theta_l$. The results also show that the variance of $\Delta\dot\delta$ increases modestly with P_d as the system approaches the bifurcation. Unlike the SMIB system, the variance of ΔV_l is a good early warning sign of the bifurcation. It is also much more sensitive to the increase of P_d compared to $\Delta\delta - \Delta\theta_l$ and $\Delta\dot\delta$.

B. Discussion

As was the case with the SMIB system, when the power flowing on the transmission line in this system reaches its transfer limit, the algebraic equations become singular. However, unlike the previous system, the differential equations of this system do not become singular at the bifurcation point of the algebraic equations. Fig. 9 shows the sample trajectories of the two systems' rotor angles. Both signals are Gaussian stochastic processes. The rotor angle in the SMIB system is an Ornstein-Uhlenbeck process while the rotor angle in the SMSL system varies like the position of the brownian particle [40]. The existence of the infinite bus in the former system causes this difference.

One difference between the SMSL system and the SMIB system is the absence of the term comprising $\Delta\delta$ in (50) compared with (5). This causes the linearized state matrix to be independent of the bifurcation parameter. From (43), one can show that the normalized autocorrelation of $\Delta\dot\delta$ depends only on A and the time lag. Since A is state-independent in this
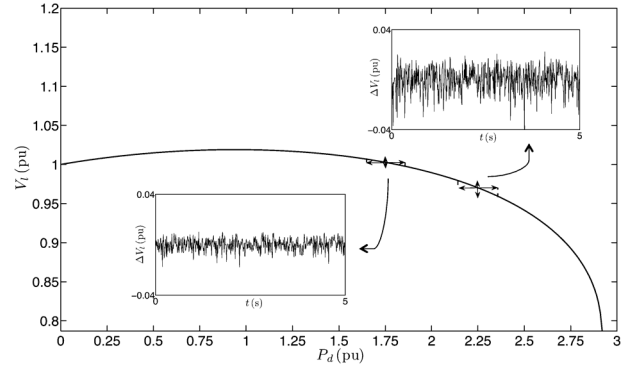

Fig. 10.   The load bus voltage as a function of load power. The load bus voltage magnitude becomes increasingly sensitive to power fluctuations as the system approaches the bifurcation. This increased sensitivity raises the voltage magnitude's variance.
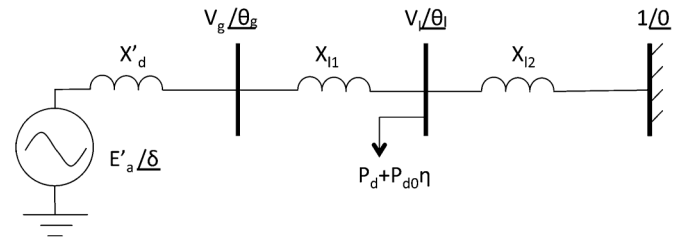

Fig. 11.   Three-bus system.

system, the autocorrelation of $\Delta\dot\delta$ will be constant for a specific Δt.

The increase of the variances of both differential and algebraic variables is due to the non-linearity of the algebraic equations. Fig. 10 shows that as the load power increases, the perturbation of the load power causes a larger deviation in the load busbar voltage magnitude. Consequently, variance of this algebraic variable increases with P_d. Likewise, this nonlinearity causes the coefficient C_5 in (50) to increase as the load power is increased, increasing the variance of $\Delta\dot\delta$.

While voltage variance increases with load, this system does not technically show CSD before the bifurcation, since increases in both variance and autocorrelation are essential to conclude that CSD has occurred [9]. Also, the eigenvalues of the state matrix of this system do not vary with load. This confirms that CSD does not occur in this system, since the poles of the dynamical system do not move toward the right-half plane as the bifurcation parameter increases [1], [9].

V. THREE-BUS SYSTEM

Real power systems have properties that are common to both the SMIB in Section III and the SMSL in Section IV. In order to explore CSD for a system that has both an infinite bus, and the potential for voltage collapse case, this section looks at the three-bus system in Fig. 11.

A. Model and Results

The three-bus system consists of a generator connected to a load bus through a transmission line, which is connected to an infinite bus through another transmission line. In the SMIB system, the bifurcation occurred in the differential equations. Increasing the load in the three-bus system causes a saddle-node bifurcation in the algebraic equations $F_1(\delta, \underline{y}, 0) = 0, \underline{F_2}(\delta, \underline{y}, 0) = 0$ (in terms of (1), (2)), as in the
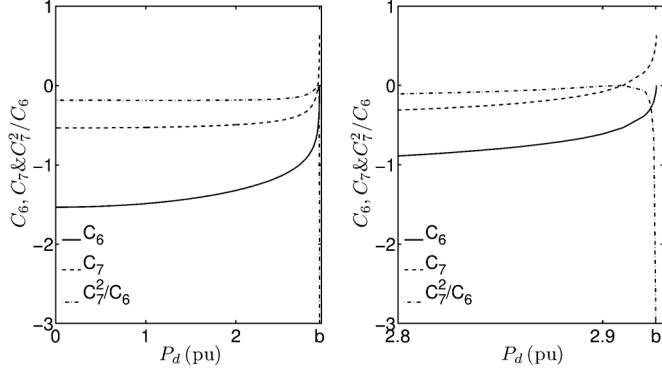
Fig. 12. Three variables C_6, C_7 and C_7^2/C_6 derived by linearizing the Three-bus system model. The left panel shows the variables versus P_d for Case B. The right panel shows a close-up view of the variables near the bifurcation. Note that as $P_d \rightarrow P_{d,cr}$, $C_6 \rightarrow 0$ while C_7 approaches a finite value of ~ 0.6. $C_7^2/C_6 \rightarrow \infty$, as $P_d \rightarrow P_{d,cr}$.

SMSL system. However, unlike in the SMSL system, the bifurcation in these algebraic equations also causes a bifurcation in the differential (5).

We studied this system for two different cases. Our goal in studying these two cases was to show that the CSD signs for some variables can vary differently with changing the system parameters. In case A, the parameters of this system are similar to those in the SMIB system except for the following:

$$X_{l1} = 0.1 \text{ pu}, \ X_{l2} = 0.35 \text{ pu}, \ X_d' = 0.1 \text{ pu}$$

In Case B, the following parameters were used:

$$X_{l1} = 0.3 \text{ pu}, \ D = 0.001 \ \frac{\text{pu}}{\text{rad/s}}$$

The algebraic equations of the three-bus system are as follows:

$$\frac{\left(\frac{E_a' V_l}{X} \sin(\delta - \theta_l) - \frac{2}{3} P_d\right)}{M} = 0 \tag{52}$$

$$\frac{E_a' V_l}{X} \sin(\delta - \theta_l) - \frac{V_l}{X_{l2}} \sin(\theta_l) - P_{d0}\eta = P_d \tag{53}$$

$$\frac{E_a' V_l}{X} \cos(\delta - \theta_l) + \frac{V_l}{X_{l2}} \cos(\theta_l) = V_l^2 \cdot \left(\frac{1}{X} + \frac{1}{X_{l2}}\right) \tag{54}$$

where $X = X_d' + X_{l1}$, V_l, θ_l are voltage magnitude and angle of the load busbar. Equation (52) is equivalent to $F_1(\delta, \underline{y}, 0)$ in (1), and (53), (54), which are the simplified active and reactive power flow equations at the load busbar, are equivalent to $F_2(\delta, \underline{y}, 0)$ in (2). We assumed that $P_{g0} = 2P_d/3$, which is reflected in (52).

The following equalities relate this system to the general model in (5):

$$\gamma = \frac{D}{2M}; \ \omega_0^2 = \frac{-C_6}{M}; \ f = \frac{-C_7}{M} \tag{55}$$

where C_6 and C_7 are functions of the system state at the equilibrium point. The derivation and expressions for C_6, C_7 are presented in Appendix B. Fig. 12 shows C_6, C_7 versus P_d. When the load increases, C_6 approaches 0, and a bifurcation in the differential equation (5) and (55) occurs.
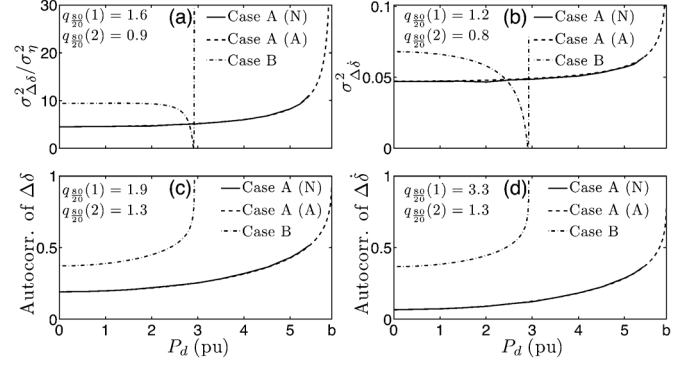

Fig. 13. Panels a,b show the variances of $\Delta\delta, \Delta\dot{\delta}$ versus load power (P_d). Panels c,d show the autocorrelations of $\Delta\delta, \Delta\dot{\delta}$ versus P_d. The ratios $q_{80/20}(1), q_{80/20}(2)$ are for case A, case B respectively. CaseA(N), CaseA(A) denote numerical and analytical solutions for case A.
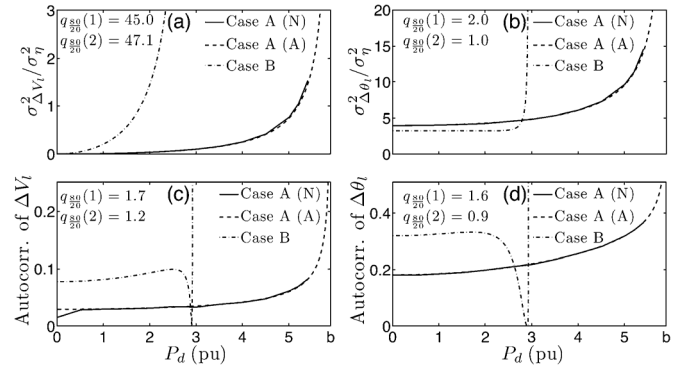

Fig. 14. Panels a,b show the variances of $\Delta V_l, \Delta\theta_l$ versus P_d. Panels c,d show the autocorrelations of $\Delta V_l, \Delta\theta_l$ versus P_d.

Using (55), the expressions in Section II-B, and (76), (77) in Appendix B, we calculated the variances and autocorrelations of $\Delta\delta, \Delta\dot{\delta}, \Delta V_l$ and $\Delta\theta_l$. We chose the autocorrelation time lag Δt of the variables to be equal to 0.14 s taking a similar approach as in Section III-B. Although the chosen Δt may not be optimal for all of the variables, it represents a reasonable compromise between simplicity (choosing just one Δt) and usefulness as early warning signs. Figs. 13, 14 compare the analytical solutions with the numerical solutions of the variances and autocorrelations of $\Delta\delta, \Delta\dot{\delta}, \Delta V_l$ and $\Delta\theta_l$.

Fig. 13 shows that although the growth rates of the autocorrelations of $\Delta\delta, \Delta\dot{\delta}$ are not large, the autocorrelations increase monotonically in both cases. As mentioned in Section III-C, it is possible to have larger indicators (growth ratios) by subtracting a bias value from the autocorrelations. On the other hand, the variances of $\Delta\delta, \Delta\dot{\delta}$ in Fig. 13, do not monotonically increase for case B. We will explain this behavior in the next subsection. As a result, they are not reliable indicators of proximity to the bifurcation.

Fig. 14 shows that although both variances of ΔV_l and $\Delta\theta_l$ increase with P_d, increase of the variance of ΔV_l is more significant. Also, the variance of $\Delta\theta_l$ does not increase monotonically with P_d for case B. As a result, the variance of ΔV_l seems to be a better indicator of the system stability.

In Fig. 14, the autocorrelation of ΔV_l until very near the bifurcation is small compared to those in Fig. 13. This is caused by C_{26} being very small in (76), so ΔV_l is tied to the differential variables weakly. As a result, ΔV_l behaves in part like

η—the white random variable, and hence its autocorrelation is not a good indicator of proximity to the bifurcation. In addition, nonmonotonicity of the autocorrelations of ΔV_l, $\Delta \theta_l$ for case B in Fig. 14 shows that they are not good early warning signs of bifurcation.

B. Discussion

After studying this system with a range of different parameters, we found that autocorrelations of the differential variables and variance of the voltage magnitude are consistently good indicators of proximity to the bifurcation.

On the other hand, as shown in Fig. 13, variance in the differential variables is not a reliable indicator. Namely, variances change non-monotonically (i.e., they do not always increase) and, importantly, may exhibit very abrupt changes. Fig. 12 provides some clues as to the reason for this latter phenomenon. In this figure, the absolute value of C_7 decreases with P_d and becomes zero very close to the bifurcation point, at $P_{d|C_7=0}$. Therefore, the variances of $\Delta \delta$ and $\Delta \dot{\delta}$, which are proportional to C_7^2, decrease and vanish at $P_{d|C_7=0}$. Past this point, $|C_7|$ increases, while C_6 continues to decrease and vanishes at b. Therefore, the variances of $\Delta \delta$ and $\Delta \dot{\delta}$, which are proportional to C_7^2/C_6, increase to infinity in the very narrow interval $(P_{d|C_7=0}, b)$; see Fig. 12. This explains the sharp features in Figs. 13(a), 13(b); a similar explanation can be given to such a feature in Figs. 14(c), 14(d). Therefore, neither the variances of $\Delta \delta$, $\Delta \dot{\delta}$ or the autocorrelations of ΔV_l, $\Delta \theta_l$ are good indicators of proximity to bifurcation.

The results for this system clearly show that not all of the variables in a power system will show CSD signs long before the bifurcation. Although autocorrelations and variances of all variables increase before the bifurcation, some of them increase only very near the bifurcation or the increase is not monotonic. Hence, these variables are not useful indicators of proximity to the bifurcation. In the three-bus system, autocorrelation in the differential equations was a better indicator of proximity than autocorrelation in ΔV_l or $\Delta \theta_l$, which are not directly associated with the differential equations. Also, ΔV_l was the only variable whose variance shows a gradual and monotonic increase with the bifurcation parameter.

VI. CSD IN MULTI-MACHINE SYSTEMS

In order to compare these analytical results to results from more practical power system, this section presents numerical results for two multi-machine systems.

The first system was similar to the Three-bus system (case B in Section V). The only difference was that instead of infinite bus, a generator similar to the other generator was used. The numerical simulation results were similar to the Three-bus system, except for the autocorrelation of $\Delta \dot{\delta}$. Fig. 15 shows that the autocorrelation of $\Delta \dot{\delta}$ increases for one of the machines, while it decreases for the other one. This shows that the autocorrelation of $\Delta \dot{\delta}$ is not a reliable indicator of the proximity to the bifurcation in this system.

The second system we studied was the New England 39-bus system, using the system data from [41] We simulated this system for different load levels using the power system analysis toolbox (PSAT) [42]. In order to change the system loading, each load was multiplied by the same factor. At each load
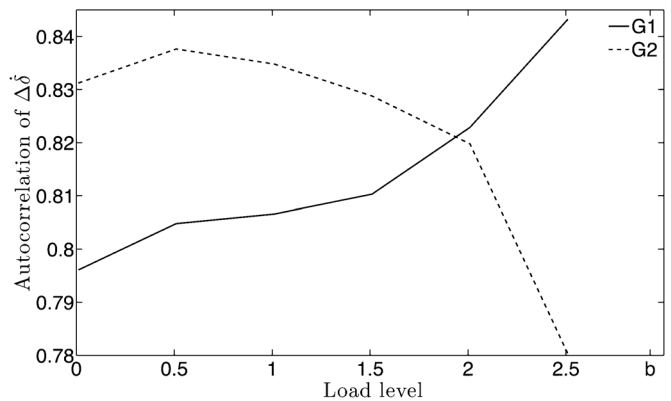

Fig. 15. Autocorrelation of $\Delta \dot{\delta}$ for two machines in the Three-bus system with two generators. G_1 is the same generator as in the Three-bus system and G_2 is the new generator.
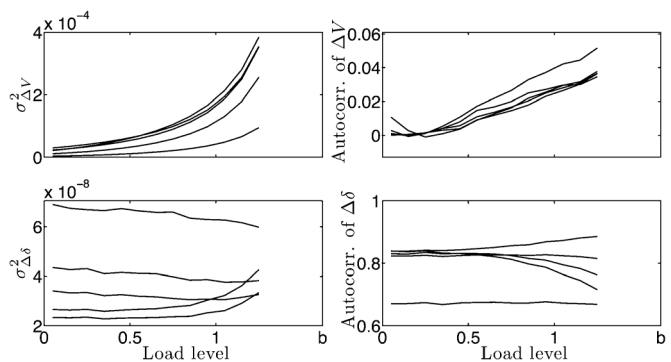

Fig. 16. The variances and autocorrelations of five bus voltage magnitudes and five generator rotor angles of the 39-bus system. Load level is the ratio of the values of the system's loads to their nominal values.

level, we added white noise to each load. As one would expect, increasing the loads moves the system towards voltage collapse. For solving the stochastic DAEs, we used the fixed-step trapezoidal solver of PSAT with the step size of 0.01 s. The noise intensity was kept constant for all load levels.

The simulation results show that the variances and autocorrelations of bus voltage magnitudes increase with load. However, similar to the Three-bus system, the autocorrelations of voltage magnitudes are very small, indicating that in practice, these variables would not be good indicators of proximity. The variances and autocorrelations of generator rotor angles and speeds and bus voltage angles did not consistently show an increasing pattern. Fig. 16 shows the variances and autocorrelations of the voltage magnitudes of five buses and the rotor angles of five generators of the system. The buses and generators were arbitrarily chosen. As in previous results, the autocorrelation time lag was chosen to be 0.1 s.

The results in this section suggest that autocorrelations of differential variables show nonmonotonic behavior in some cases, which limits their application as early waning signs of bifurcation.

Exciters, governors and frequency-dependent loads were not included in the results shown here. However, tests with exciters and governors indicated that that adding these elements to the simulations did not substantially change the conclusions. Considering the frequency-dependence of loads raised the rate at which the autocorrelation of voltage magnitudes increased. On the other hand, it decreased the rate of increase of the variance

TABLE I
THE LARGEST INDICES $q_{80/20}$ (FOR VARIANCE) AND THE RELATIVE ACTIVITY
IN THE DOMINANT MODE FOR BUS VOLTAGE MAGNITUDES

Bus	$q_{\frac{80}{20}}$ (Variance)	relative activity
38	11.5944	0.0135
29	9.9317	0.0147
28	9.0663	0.0147
33	8.5141	0.0101
37	8.3509	0.007

of voltage magnitudes. Nevertheless, the rate of increase of variance remained still significant. In this case, variance and autocorrelation of voltage magnitudes provide useful early warning of the bifurcation. In contrast, variances and autocorrelations of other variables do not provide a consistent early warning.

Comparing the measure $q_{80/20}$ for variances and autocorrelations of voltage magnitudes shows that some variables at some buses have larger growth ratios than others. As suggested in [7], [8], this may be associated with the contribution of the variables to the leading mode near the threshold of collapse. However, except for cases that are very close to (~1% away) the bifurcation, eigenvalue analysis shows that there are several simultaneously dominant modes. The results indicate that the mode whose damping decreases the fastest is most strongly connected to the variance of bus voltages. Table I shows that, in general, the buses with the largest increases in variances have larger activity in the dominant mode. On the other hand, autocorrelations do not show a similar pattern. While the exact reasons for this are not yet clear, Fig. 3 and the analytical results indicate that the autocorrelation functions of variables can take many different shapes, which affects the growth ratio of their autocorrelations.

Table I shows the buses with the highest $q_{80/20}$ indices for bus voltage variance, as well as the relative activity of these bus voltage magnitudes in the dominant mode. In order to calculate the relative activity of the bus voltages in the dominant mode, we first calculated the right modal matrix of the state matrix. Then, using a matrix which relates the differential and algebraic variables, we calculated the matrix that relates the algebraic variables and the system modes. The entries of each column of this matrix gives the relative activity of the algebraic variables in one of the modes. It should be noted that the entries shown in Table I are a small subset of the entries of the column corresponding to the dominant mode, which is why their values are so small.

In many ways, this test case is a multi-machine version of the SMSL system. As with the SMSL and Three-bus systems, variances of bus voltage magnitudes are good early warning signs. However, unlike in the SMSL system, autocorrelation in voltage magnitudes increases, albeit only slightly in some cases, with system load. Unlike in the SMSL system, voltage magnitudes in the 39-bus case have non-zero autocorrelation for $\Delta t > 0$. This results from the fact that voltage magnitudes are coupled to the differential variables in this system.

Results from this system, as with the SMSL system, suggest that variance in voltage magnitudes is a useful early warning sign of voltage collapse. It is less clear from these results if changes in autocorrelation will be sufficiently large to provide a reliable early warning of criticality.

One important point about the numerical results presented in this paper is that these results are averages over many simulations with randomly chosen sequences of η. This averaging is
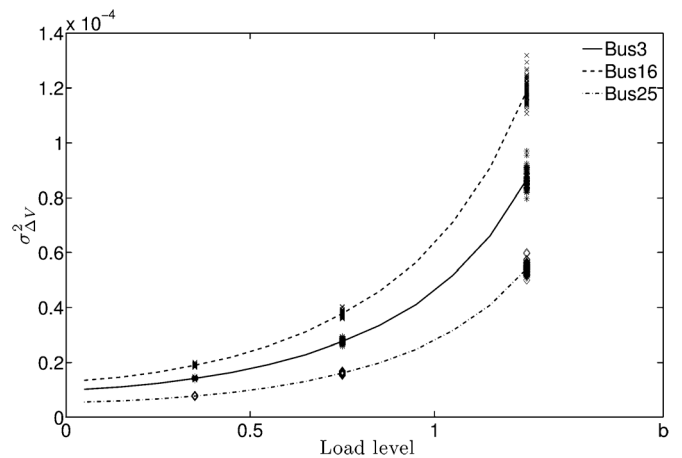

Fig. 17. Variances of three bus voltages versus load level. For three load levels, variances for 100 realizations are shown. For other load levels, only mean of the variances are shown.

different from the quantities observed by power system operators. One should take this into account when using CSD signs for monitoring system stability. For example, Fig. 17 shows the variances of the voltage magnitudes of three buses in the 39-bus system. For each bus, mean variances (for 100 realizations) are shown for all load levels. For three load levels (low, medium and high load level), the actual measured variance from each of the 100 realizations (one minute windows) is also shown. The increases in voltage magnitude variance are significant in that there is no overlap between the variances at these three load levels even for a single realization. Therefore, we conclude that, at least given the assumptions underlying these simulations, it is possible to accurately estimate the distance to bifurcation based on the variance of a one-minute stream of voltage magnitude data.

VII. CONCLUSION

In this paper, we analytically and numerically solve the stochastic differential algebraic equations for three small power system models in order to understand critical slowing down in power systems. The results from the single machine infinite bus system and the Three-bus system models show that critical slowing down does occur in power systems, and illustrate that autocorrelation and variance in some cases can be good indicators of proximity to criticality in power systems. The results also show that the way in which the bifurcation parameter changes the system state matrix (A) importantly influences the observed changes in autocorrelation and variance. For example, the constant state matrix in the single machine single load system (see (7), (51)) caused the autocorrelation of the differential variable to be constant. On the other hand, in the SMIB and Three-bus systems, the state matrix changed with the the bifurcation parameter; that is, the coefficient ω_0 in (7) changed with the bifurcation parameter P_m (for SMIB, see (28), (29)) or P_d (Three-bus, see (55)). As a result, the variance and autocorrelation of the differential variables changed with the bifurcation parameter, and in some cases indicate proximity to bifurcation.

Although the signs of critical slowing down do consistently appear as the systems approach bifurcation, only in a few of the variables did the increases in autocorrelation appear sufficiently early to give a useful early warning of potential collapse. On the other hand, variance in load bus voltages consistently

showed substantial increases with load, indicating that variance in bus voltages can be a good indicator of voltage collapse in multi-machine power system models. This was verified for the New England 39-bus system. Determining intuitive analytical or physical explanations for why some variables show the signs of CSD better than others requires additional investigation, and is a subject for future research.

Together these results suggest that it is possible to obtain useful information about system stability from high-sample rate time-series data, such as that produced by synchronized phasor measurement units. Future research will focus on developing an effective power system stability indicator based on these results.

APPENDIX A

The derivation of (50) is presented in this section. By linearizing (45) around the equilibrium and replacing the obtained equation for P_g in (44), we obtained the following:

$$M\Delta\ddot{\delta} + D\Delta\dot{\delta} = -C_{12}\Delta V_l - C_{13}(\Delta\delta - \Delta\theta_l) \qquad (56)$$

where C_{12} and C_{13} are:

$$C_{12} = E'_a|Y_{gl}|\sin(\theta_{l0} - \delta_0 - \pi/2 + \phi_{gl}) \qquad (57)$$
$$C_{13} = V_{l0}E'_a|Y_{gl}|\cos(\theta_{l0} - \delta_0 - \pi/2 + \phi_{gl}) \qquad (58)$$

where $|Y_{gl}| = \sqrt{G_{gl}^2 + B_{gl}^2}, \phi_{gl} = \arctan(B_{gl}/G_{gl})$. By linearizing (48) and (49) around the equilibrium and solving for ΔV_l and $\Delta\delta - \Delta\theta_l$, we obtained the following:

$$\Delta V_l = C_{14} \qquad (59)$$
$$\Delta\delta - \Delta\theta_l = C_{15} \qquad (60)$$

where C_{14} and C_{15} are:

$$\begin{bmatrix} C_{14} \\ C_{15} \end{bmatrix} = \frac{\begin{bmatrix} C_{19}P_{d0} - C_{17}Q_{d0} \\ C_{18}P_{d0} - C_{16}Q_{d0} \end{bmatrix}}{(C_{17}C_{18} - C_{16}C_{19})} \qquad (61)$$

where $C_{16} - C_{19}$ are given below:

$$C_{16} = E'_a|Y_{gl}|\sin(\theta_{l0} - \delta_0 + \pi/2 - \phi_{gl}) + 2G_{ll}V_{l0} \quad (62)$$
$$C_{17} = V_{l0}E'_a|Y_{gl}|\cos(\theta_{l0} - \delta_0 + \pi/2 - \phi_{gl}) \qquad (63)$$
$$C_{18} = -E'_a|Y_{gl}|\cos(\theta_{l0} - \delta_0 + \pi/2 - \phi_{gl}) - 2B_{ll}V_{l0} \qquad (64)$$
$$C_{19} = V_{l0}E'_a|Y_{gl}|\sin(\theta_{l0} - \delta_0 + \pi/2 - \phi_{gl}) \qquad (65)$$

Using (59) and (60), we rewrote (56) as (50) where C_5 is:

$$C_5 = \frac{(C_{13}C_{18} + C_{12}C_{19})P_{d0} - (C_{13}C_{16} + C_{12}C_{17})Q_{d0}}{C_{16}C_{19} - C_{17}C_{18}} \qquad (66)$$

APPENDIX B

The derivation of C_6, C_7 is presented in this section. By using (1) and linearizing (52)–(54) around the equilibrium, we have the following:

$$\Delta\ddot{\delta} = -\left(D\Delta\dot{\delta} + C_{20}\Delta V_l + C_{21}(\Delta\delta - \Delta\theta_l)\right)/M \quad (67)$$
$$0 = -P_{d0}\eta + C_{22}\Delta V_l + C_{21}\Delta\delta + C_{23}\Delta\theta_l \qquad (68)$$
$$0 = -\Delta V_l + C_{24}\Delta\delta + C_{25}\Delta\theta_l \qquad (69)$$

where C_{20} through C_{25} are as follows:

$$C_{20} = \frac{E'_a}{X}\sin(\delta_0 - \theta_{l0}) \qquad (70)$$
$$C_{21} = \frac{E'_a V_{l0}}{X}\cos(\delta_0 - \theta_{l0}) \qquad (71)$$
$$C_{22} = C_{20} - \sin(\theta_{l0})/X_{l2} \qquad (72)$$
$$C_{23} = -C_{21} - \frac{V_{l0}}{X_{l2}}\cos(\theta_{l0}) \qquad (73)$$
$$C_{24} = -\beta E'_a\sin(\delta_0 - \theta_{l0}) \qquad (74)$$
$$C_{25} = -C_{24} - (1 - \beta)\cdot\sin(\theta_{l0}) \qquad (75)$$

where $\beta = X_{l2}/(X + X_{l2})$. Using (68) and (69), we solved for ΔV_l and $\Delta\theta_l$:

$$\Delta V_l = C_{26}\Delta\delta + C_{27}\eta \qquad (76)$$
$$\Delta\theta_l = C_{28}\Delta\delta + C_{29}\eta \qquad (77)$$

where C_{26} through C_{29} are as follows:

$$\begin{bmatrix} C_{26} \\ C_{27} \\ C_{28} \\ C_{29} \end{bmatrix} = \frac{\begin{bmatrix} C_{23}C_{24} - C_{21}C_{25} \\ C_{25}P_{d0} \\ -C_{21} - C_{22}C_{24} \\ P_{d0} \end{bmatrix}}{(C_{22}C_{25} + C_{23})} \qquad (78)$$

Equations (67), (76)–(78) lead to the following expressions:

$$C_6 = C_{21}C_{28} - C_{20}C_{26} - C_{21} \qquad (79)$$
$$C_7 = C_{21}C_{29} - C_{20}C_{27} \qquad (80)$$

ACKNOWLEDGMENT

REFERENCES

[1] M. Scheffer, J. Bascompte, W. A. Brock, V. Brovkin, S. R. Carpenter, V. Dakos, H. Held, E. H. Van Nes, M. Rietkerk, and G. Sugihara, "Early-warning signals for critical transitions," *Nature*, vol. 461, no. 7260, pp. 53–59, Sep. 2009.

[2] T. Lenton, V. Livina, V. Dakos, E. Van Nes, and M. Scheffer, "Early warning of climate tipping points from critical slowing down: Comparing methods to improve robustness," *Philos. Trans. Royal Soc. A: Math., Phys. Eng. Sci.*, vol. 370, no. 1962, pp. 1185–1204, 2012.

[3] V. Dakos, M. Scheffer, E. H. Van Nes, V. Brovkin, V. Petoukhov, and H. Held, "Slowing down as an early warning signal for abrupt climate change," *Proc. Natl. Acad. Sci.*, vol. 105, no. 38, pp. 14 308–14 312, Sep. 2008.

[4] V. Dakos, S. Kéfi, M. Rietkerk, E. H. van Nes, and M. Scheffer, "Slowing down in spatially patterned ecosystems at the brink of collapse," *Amer. Natur.*, vol. 177, no. 6, pp. E153–E166, 2011.

[5] B. Litt, R. Esteller, J. Echauz, M. D'Alessandro, R. Shor, T. Henry, P. Pennell, C. Epstein, R. Bakay, and M. Dichter *et al.*, "Epileptic seizures may begin hours in advance of clinical onset: A report of five patients," *Neuron*, vol. 30, no. 1, pp. 51–64, 2001.

[6] E. Cotilla-Sanchez, P. Hines, and C. Danforth, "Predicting critical transitions from time series synchrophasor data," *IEEE Trans. Smart Grid*, vol. 3, no. 4, pp. 1832–1840, Dec. 2012.

[7] D. Podolsky and K. Turitsyn, "Random load fluctuations and collapse probability of a power system operating near codimension 1 saddle-node bifurcation," in *IEEE Power and Energy Soc. General Meeting (PES)*, 2013.

[8] D. Podolsky and K. Turitsyn, Critical Slowing-Down as Indicator of Approach to the Loss of Stability arXiv preprint arXiv:1307.4318, Jul. 2013.

[9] C. Kuehn, "A mathematical framework for critical transitions: Bifurcations, fast-slow systems and stochastic dynamics," *Phys. D: Nonlinear Phen.*, vol. 240, no. 12, pp. 1020–1035, Jun. 2011.

[10] M. C. Boerlijst, T. Oudman, and A. M. de Roos, "Catastrophic collapse can occur without early warning: Examples of silent catastrophes in structured ecological models," *PLOS ONE*, vol. 8, no. 4, p. e62033, 2013.

[11] A. Hastings and D. B. Wysham, "Regime shifts in ecological systems can occur with no warning," *Ecology Lett.*, vol. 13, no. 4, pp. 464–472, 2010.

[12] I. Dobson, "Observations on the geometry of saddle node bifurcation and voltage collapse in electrical power systems," *IEEE Trans. Circuits Syst. I, Fundam. Theory Appl.*, vol. 39, no. 3, pp. 240–243, Mar. 1992.

[13] C. A. Canizares *et al.*, "Voltage stability assessment: Concepts, practices and tools," in *Power Syst. Stability Subcommittee Special Publication IEEE/PES*, 2002.

[14] V. Ajjarapu and B. Lee, "Bifurcation theory and its application to nonlinear dynamical phenomena in an electrical power system," *IEEE Trans. Power Syst.*, vol. 7, no. 1, pp. 424–431, Feb. 1992.

[15] C. A. Cañizares, N. Mithulananthan, F. Milano, and J. Reeve, "Linear performance indices to predict oscillatory stability problems in power systems," *IEEE Trans. Power Syst.*, vol. 19, no. 2, pp. 1104–1114, May 2004.

[16] R. Avalos, C. Canizares, F. Milano, and A. Conejo, "Equivalency of continuation and optimization methods to determine saddle-node and limit-induced bifurcations in power systems," *IEEE Trans. Circuits Syst. I, Reg. Papers*, vol. 56, no. 1, pp. 210–223, Jan. 2009.

[17] G. Revel, A. Leon, D. Alonso, and J. Moiola, "Bifurcation analysis on a multimachine power system model," *IEEE Trans. Circuits Syst. I, Reg. Papers*, vol. 57, no. 4, pp. 937–949, Apr. 2010.

[18] H. D. Chiang, I. Dobson, R. J. Thomas, J. S. Thorp, and L. Fekih-Ahmed, "On voltage collapse in electric power systems," *IEEE Trans. Power Syst.*, vol. 5, no. 2, pp. 601–611, 1990.

[19] M. M. Begovic and A. G. Phadke, "Control of voltage stability using sensitivity analysis," *IEEE Trans. Power Syst.*, vol. 7, no. 1, pp. 114–123, 1992.

[20] M. Glavic and T. Van Cutsem, "Wide-area detection of voltage instability from synchronized phasor measurements. Part I: Principle," *IEEE Trans. Power Syst.*, vol. 24, no. 3, pp. 1408–1416, Aug. 2009.

[21] C. De Marco and A. Bergen, "A security measure for random load disturbances in nonlinear power system models," *IEEE Trans. Circuits Syst.*, vol. 34, no. 12, pp. 1546–1557, Dec. 1987.

[22] C. Nwankpa, S. Shahidehpour, and Z. Schuss, "A stochastic approach to small disturbance stability analysis," *IEEE Trans. Power Syst.*, vol. 7, no. 4, pp. 1519–1528, Nov. 1992.

[23] M. Anghel, K. A. Werley, and A. E. Motter, "Stochastic model for power grid dynamics," in *Proc. IEEE 40th Annual Hawaii Intl. Conf. Syst. Sci.*, Jan. 2007.

[24] Z. Y. Dong, J. H. Zhao, and D. Hill, "Numerical simulation for stochastic transient stability assessment," *IEEE Trans. Power Syst.*, vol. 27, no. 4, pp. 1741–1749, Nov. 2012.

[25] K. Wang and M. L. Crow, "The Fokker-Planck equation for power system stability probability density function evolution," *IEEE Trans. Power Syst.*, vol. 28, no. 3, pp. 2994–3001, Aug. 2013.

[26] S. Dhople, Y. Chen, L. DeVille, and A. Dominguez-Garcia, "Analysis of power system dynamics subject to stochastic power injections," *IEEE Trans. Circuits Syst. I, Reg. Papers*, vol. 60, no. 12, pp. 3341–3353, Dec. 2013.

[27] F. Milano and R. Zarate-Minano, "A systematic method to model power systems as stochastic differential algebraic equations," *IEEE Trans. Power Syst.*, vol. 28, no. 4, pp. 4537–4544, Nov. 2013.

[28] S. Abraham and J. Efford, Eds., Final Report on the August 14, 2003 Blackout in the United States and Canada: Causes and Recommendations US-Canada Power Syst. Outage Task Force, Tech. Rep., 2004.

[29] "Arizona-Southern California Outages on September 8, 2011: Causes and Recommendations," FERC and NERC Staff, Apr. 2012, Tech. Rep..

[30] M. Chertkov, S. Backhaus, K. Turitsyn, V. Chernyak, and V. Lebedev, "Voltage Collapse and ODE Approach to Power Flows: Analysis of a Feeder Line With Static Disorder in Consumption/Production," arXiv preprint arXiv:1106.5003, 2011.

[31] G. Ghanavati, P. D. H. Hines, T. I. Lakoba, and E. Cotilla-Sanchez, "Calculation of the autocorrelation function of the stochastic single machine infinite bus system," in *Proc. North American Power Symp.*, Sep. 2013.

[32] A. J. F. Hauer, D. J. Trudnowski, and J. G. DeSteese, "A perspective on WAMS analysis tools for tracking of oscillatory dynamics," in *Proc. IEEE Power Energy Soc. General Meeting (PES)*, Jun. 2007, pp. 1–10.

[33] C. W. Gardiner, *Stochastic Methods: A Handbook for the Natural and Social Sciences*, 4th ed. Berlin, Germany: Springer, 2010.

[34] R. L. Stratonovich, *Introduction to the Theory of Random Noise.* : Gordon and Breach, 1963.

[35] P. Blanchard, R. L. Devaney, and G. R. Hall, *Differential Equations.* : Thomson Brooks/Cole, 2006.

[36] F. P. Demello and C. Concordia, "Concepts of synchronous machine stability as affected by excitation control," *IEEE Trans. Power Apparatus Syst.*, no. 4, pp. 316–329, 1969.

[37] Y. Wang, D. J. Hill, R. H. Middleton, and L. Gao, "Transient stability enhancement and voltage regulation of power systems," *IEEE Trans. Power Syst.*, vol. 8, no. 2, pp. 620–627, 1993.

[38] D. Wei and X. Luo, "Noise-induced chaos in single-machine infinite-bus power systems," *EPL (Europhysics Lett.)*, vol. 86, no. 5, p. 50 008, 2009, 6 pp.

[39] P. Kundur, N. J. Balu, and M. G. Lauby, *Power System Stability and Control*, 1st ed. New York, USA: McGraw-hill, 1994.

[40] W. Horsthemke and R. Lefever, *Noise-Induced Transitions*, 2nd ed. Berlin: Springer, 2006.

[41] M. Pai, *Energy Function Analysis for Power System Stability*, 1st ed. Norwell, MA, USA: Kluwer Academic, 1989.

[42] F. Milano, "An open source power system analysis toolbox," *IEEE Trans. Power Syst.*, vol. 20, no. 3, pp. 1199–1206, 2005.

[43] W. Rümelin, "Numerical treatment of stochastic differential equations," *SIAM J. Numer. Anal.*, pp. 604–613, 1982.

[44] Y. Susuki and I. Mezic, "Nonlinear koopman modes and a precursor to power system swing instabilities," *IEEE Trans. Power Syst.*, vol. 27, no. 3, pp. 1182–1191, 2012.

[45] A. J. Veraart, E. J. Faassen, V. Dakos, E. H. van Nes, M. Lürling, and M. Scheffer, "Recovery rates reflect distance to a tipping point in a living system," *Nature*, vol. 481, no. 7381, pp. 357–359, 2011.

[46] I. Dobson, "The irrelevance of load dynamics for the loading margin to voltage collapse and its sensitivities," in *Proc. ECC/NSF Workshop Bulk Power Syst. Voltage Phenom. III, Voltage Stability, Security & Control*, Davos, Switzerland, 1994.

[47] A. Bergen and V. Vittal, *Power systems analysis*, 2nd ed. Englewood Cliffs, NJ, USA: Prentice Hall, 1999.

[48] I. Dobson and H. D. Chiang, "Towards a theory of voltage collapse in electric power systems," *Syst. Control Lett.*, vol. 13, no. 3, pp. 253–262, Sep. 1989.

[49] H. G. Kwatny, R. F. Fischl, and C. O. Nwankpa, "Local bifurcation in power systems: Theory, computation, application," *Proc. IEEE*, vol. 83, no. 11, pp. 1456–1483, Nov. 1995.

[50] P. D. H. Hines, E. Cotilla-Sanchez, B. O'hara, and C. Danforth, "Estimating dynamic instability risk by measuring critical slowing down," in *Proc. IEEE Power Energy Soc. General Meeting*, 2011, pp. 1–5.

[51] R. Mannella and V. Peter, "Itô versus Stratonovich: 30 years later," *Fluct. Noise Lett.*, vol. 11, no. 01, p. 1240010, Mar. 2012.

[52] S. Ayasun, C. Nwankpa, and H. Kwatny, "Computation of singular and singularity induced bifurcation points of differential-algebraic power system model," *IEEE Trans. Circuits Syst. I, Reg. Papers*, vol. 51, no. 8, pp. 1525–1538, Aug. 2004.

[53] W. Coffey, Y. Kalmykov, and J. Waldron, *The Langevin Equation: With Applications in Physics, Chemistry, Electrical Engineering*, ser. World Scientific series in contemporary physics, 2nd ed. Singapore: World Scientific, 2004 [Online]. Available: http://books.google.com/books?id=AlzSLSOAJK4C

[54] T. Van Cutsem, "Voltage instability: Phenomena, countermeasures, analysis methods," *Proc. IEEE*, vol. 88, no. 2, pp. 208–227, Feb. 2000.

[55] G. Hou and V. Vittal, "Trajectory sensitivity based preventive control of voltage instability considering load uncertainties," *IEEE Trans. Power Syst.*, vol. 27, no. 4, pp. 2280–2288, Nov. 2012.

[56] P. Kundur, J. Paserba, V. Ajjarapu, G. Andersson, A. Bose, C. Canizares, N. Hatziargyriou, D. Hill, A. Stankovic, C. Taylor, T. Van Cutsem, and V. Vittal, "Definition and classification of power system stability IEEE/CIGRE joint task force on stability terms and definitions," *IEEE Trans. Power Syst.*, vol. 19, no. 3, pp. 1387–1401, Aug. 2004.

[57] C. A. Canizares, "On bifurcations voltage collapse and load modeling," *IEEE Trans. Power Syst.*, vol. 10, no. 1, pp. 512–522, February 1995.

Goodarz Ghanavati (S'11) received the B.S. and M.S. degrees in electrical engineering from Amirkabir University of Technology, Tehran, Iran, in 2005 and 2008, respectively. Currently, he is pursuing the Ph.D. degree in Electrical Engineering at the University of Vermont, Burlington, VT, USA.

He worked as a Design Engineer at Monenco Iran Co. His research interests include power system dynamics, stochastic modeling of power systems, phasor measurement unit applications and smart grid.

Taras I. Lakoba received the Diploma in physics from Moscow State University, Moscow, Russia, in 1989, and the Ph.D. degree in applied mathematics from Clarkson University, Potsdam, NY, USA, in 1996.

He is now an Associate Professor at the Department of Mathematics and Statistics of the University of Vermont. His research interests include the effect of noise and nonlinearity in fiber-optic communication systems, stability of numerical methods, and perturbation techniques.

Paul D. H. Hines (S'96–M'07) received the B.S. degree in 1997 from University of Washington, Seattle, WA, USA, the M.S. degree in 2001 from Seattle Pacific University, Seattle, WA, USA, both in electrical engineering, and the Ph.D. degree in 2007 in engineering and public policy from Carnegie Mellon University, Pittsburgh, PA, USA.

He is currently an Assistant Professor in the School of Engineering, and the Dept. of Computer Science at the University of Vermont, Burlington, VT, USA, and a member of the adjunct research faculty at the Carnegie Mellon Electricity Industry Center. Formerly he worked at the U.S. National Energy Technology Laboratory, the US Federal Energy Regulatory Commission, Alstom ESCA, and Black and Veatch.

Dr. Hines currently serves as the vice-chair of the IEEE Working Group on Understanding, Prediction, Mitigation and Restoration of Cascading Failures, and as an Associate Editor for the IEEE TRANSACTIONS ON SMART GRID. He is National Science Foundation CAREER award winner.

Eduardo Cotilla-Sanchez (S'08–M'12) received the M.S. and Ph.D. degrees in electrical engineering from the University of Vermont, Burlington, VT, USA, in 2009 and 2012, respectively.

He is currently an Assistant Professor in the School of Electrical Engineering and Computer Science at Oregon State University, Corvallis. His primary field of research is electrical infrastructure protection, in particular, the study of cascading outages.

Dr. Cotilla-Sanchez is a member of the IEEE Cascading Failure Working Group.